Journal of Catalysis 257 (2008) 396–402

Contents lists available at ScienceDirect

Journal of Catalysis

www.elsevier.com/locate/jcat

# Photocatalytic nonoxidative coupling of methane on gallium oxide and silica-supported gallium oxide

Leny Yuliati [a], Tadashi Hattori [a], Hideaki Itoh [b], Hisao Yoshida [a,*]

[a] Department of Applied Chemistry, Graduate School of Engineering, Nagoya University, Furo-cho, Chikusa-ku, Nagoya 464-8603, Japan
[b] Division of Environmental Research, EcoTopia Science Institute, Nagoya University, Furo-cho, Chikusa-ku, Nagoya 464-8603, Japan

ARTICLE INFO

*Article history:*
Received 22 January 2008
Revised 29 April 2008
Accepted 20 May 2008
Available online 20 June 2008

*Keywords:*
Photocatalytic nonoxidative coupling of methane
Gallium oxide photocatalyst
Silica-supported gallium oxide
Local structure

ABSTRACT

Both unsupported and silica-supported gallium oxide were found to promote the nonoxidative coupling of methane (NOCM) to produce ethane and hydrogen upon photoirradiation at around room temperature. The unsupported gallium oxide demonstrated high methane conversion and high ethane selectivity in hydrocarbon products; however, the amount of hydrogen produced was not equivalent to the amount of ethane produced, because other reactions, such as consecutive coupling and coke/carbon formation, also would proceed. The gallium content on the silica-supported gallium oxide affected both the local structure of gallium species and the photocatalytic property. The sample with the lowest loadings of Ga (0.1 mol%), on which the gallium oxide existed mainly as highly dispersed tetrahedral species, exhibited high specific activity per Ga atom and high selectivity for NOCM, where ethane and hydrogen were produced in almost equal amounts. The gallium oxide clusters or nanoparticles on the silica-supported samples with Ga loadings of 0.5–10 mol% exhibited low selectivity, likely due to the variety of the active sites.



## 1. Introduction

Being the major component of natural gas as well as a potential carbon source, methane utilization remains highly desirable. Methane also has attracted much attention as a potential hydrogen source, having the highest H/C ratio among the hydrocarbons. However, since methane is a stable molecule, effective conversion to other useful molecules and hydrogen is not easy.

Nonoxidative coupling of methane (NOCM) is a possible reaction for obtaining both ethane and hydrogen,

$$2CH_4 \rightarrow C_2H_6 + H_2, \qquad \Delta G^0{}_{298\,K} = 68.6\ \mathrm{kJ\,mol^{-1}}. \tag{1}$$

The positive and high value of Gibbs free energy, $\Delta G^0$, demonstrates that this reaction is unfavorable and difficult at low temperatures (e.g., room temperature). However, promoting this reaction selectively with a high yield at high temperatures also is difficult, because other reactions, such as methane decomposition to carbon or coke, can proceed more easily. Moreover, carbon or coke formation will lead to rapid deactivation of the catalyst.

We have proposed an alternative pathway for converting methane through NOCM at low temperatures with the aid of photoenergy and photocatalysts. We have found many kinds of photocatalysts that promote NOCM around room temperature, including silica-based photocatalysts [1–6] and supported ceria photocatalysts [7]. A general trend observed on these photocatalysts is that the highly dispersed metal oxide species on the support or the surface defects on silica act as the photocatalytic active sites for NOCM. It is noteworthy that the methane conversion in these photocatalytic systems was much higher than that at the thermodynamic equilibrium. This is one merit of the photocatalytic system. But its use is still very far from the application. Therefore, further development of an efficient photocatalyst is highly desirable. On the other hand, in contrast to the highly dispersed species photocatalysts, the famous titanium oxide semiconductor photocatalyst has been confirmed to be unsuitable for this reaction due to its low activity and/or low stability under reductive condition [1].

The use of gallium oxide as a catalyst has been increasing in recent years. Gallium oxide has been reported to be a good catalyst for many types of reactions, including aromatization of alkanes/alkenes [8–10], alkylation and isomerization of aromatics [8,11–13], methanol conversion [14–16], selective catalytic reduction (SCR) of NO [17–20], and the Diels–Alder reaction [21], where the gallium oxide was usually dispersed on silica and/or alumina supports or incorporated into zeolites. But even though gallium oxide is one of the semiconductors, its photocatalytic activity has been reported only for water-splitting [22,23] and organic decomposition [24,25].

Recently, we briefly reported on the potential ability of gallium oxide as a photocatalyst for NOCM and dry reforming of methane

* Corresponding author. Fax: +81 52 789 3178.
*E-mail address:* yoshidah@apchem.nagoya-u.ac.jp (H. Yoshida).

0021-9517/$ – see front matter 
doi:10.1016/j.jcat.2008.05.022

(DRM) [26]. In the present study, we prepared unsupported gallium oxides and a series of silica-supported gallium oxide with various amounts of gallium oxide, and investigated the structure and the photocatalytic properties for NOCM.

## 2. Experimental

### 2.1. Materials

Two samples of gallium oxide were used as the semiconductor photocatalysts. One sample, designated $Ga_2O_3$-K, was obtained commercially from Kishida Chemicals (>99.99%). The other, designated $Ga_2O_3$-P, was prepared by the precipitation method as follows. Ammonia solution was added dropwise to an aqueous solution of $Ga(NO_3)_3$ under continuous stirring at room temperature until the additional precipitate was no longer formed. The precipitate was dried at 383 K overnight and then calcined at 1073 K for 4 h. X-ray diffraction (XRD) patterns and diffuse reflectance ultraviolet–visible (DR UV–visible) spectra confirmed that both gallium oxide samples were of $\beta$-phase.

Amorphous silica as the catalyst support was prepared by a sol–gel method from $Si(OEt)_4$ [27]. After hydrolysis of the $Si(OEt)_4$, the obtained gel was dried in an oven overnight at 393 K. The dried sample was powdered and then calcined in a flow of air at 773 K for 5 h.

Silica-supported gallium oxide samples were prepared by a conventional impregnation method. The silica (2 g) was impregnated with an aqueous solution of $Ga(NO_3)_3$ (25 ml) and heated under stirring to dryness on a hot plate at 393 K. The sample was further dried in the oven overnight at 393 K, and then calcined at 773 K for 5 h. The samples were designated $Ga(x)/SiO_2$, where $x$ represents the loading amount of Ga on silica (mol%), defined as $x = n_{Ga}/(n_{Ga} + n_{Si}) \times 100\%$.

### 2.2. Photocatalytic activity test

Photocatalytic reactions were carried out similarly as in the previous studies [1–7]. The silica-supported gallium oxide sample (0.2 g) was spread on the bottom (14 $cm^2$) of a closed quartz reactor (30 $cm^3$). For the unsupported gallium oxide samples with a low specific volume, water (ca. 1 ml) was added to help the sample spread over the reactor bottom, and then the reactor was dried in the oven at 383 K overnight. Before the reaction, the sample was usually treated in 13.3 kPa of oxygen atmosphere at 1073 K for 1 h, and then evacuated at 1073 K for 1 h. In some cases, the pretreatment was carried out at 773 K. After cooling to room temperature, methane (200 μmol) was introduced to the reactor. The photoreaction was carried out at room temperature under photoirradiation typically for 3 h. A 300-W Xe lamp, emitting UV and visible light, was used as the light source. The light intensity measured at wavelengths of 220–300 nm was ca. 10 $mW\,cm^{-2}$. The gaseous products were collected and analyzed by gas chromatography (GC). The amount of hydrogen produced was measured with a thermal conductivity detector (TCD), and the amounts of hydrocarbons produced were measured with a flame ionization detector (FID). The adsorbed products were thermally desorbed, collected, and then analyzed by GC FID.

The apparent quantum yield in the range of 220–270 nm on $Ga_2O_3$-K was roughly estimated using the equation $QY(\%) = N_e/N_p \times 100$, where $N_e$ is the number of the reacted electrons under UV light irradiation and $N_p$ is the estimated number of the incident photon in the range of 220–270 nm. $N_e$ was determined from the amount of produced hydrogen, assuming that the hydrogen was produced by two electrons as follows: $2H^+ + 2e^- \rightarrow H_2$. $N_p$ was estimated from the value measured by a Si photodiode (Topcon, UVR-2 with UD-25) in the range of 220–300 nm, where the value was corrected considering the absorption band (mainly <270 nm) of $Ga_2O_3$-K.

### 2.3. Characterizations

Brunauer–Emmett–Teller (BET) specific surface areas of the samples were calculated from the adsorption of $N_2$ at 77 K. Before measurement, the sample was treated at 673 K for 30 min in a flow of He. The amount of $N_2$ adsorbed was determined by GC TCD. Powder X-ray diffraction (XRD) patterns were recorded on a Rigaku RINT 2500 diffractometer using Cu$K\alpha$ radiation (50 kV, 100 mA).

DR UV–visible spectra were recorded at room temperature on a JASCO V-550 spectrophotometer equipped with an integrating sphere covered with $BaSO_4$ using a specially designed in situ cell. $BaSO_4$ was used as the reference. Before the measurement, the sample was treated in 13.3 kPa of oxygen atmosphere at 1073 K for 1 h and evacuated at 1073 K for 1 h. Then the sample was transferred to the optical part of the cell without being exposed to the atmosphere.

Phosphorescence spectra were recorded at 77 K on a Hitachi F-4500 fluorescence spectrophotometer with an attachment for phosphorescence measurement, using a UV-cut filter ($\lambda_{transmittance} > 330$ nm) to remove the scattered light from the light source. The sample was pretreated with 13.3 kPa of oxygen at 1073 K in a specially designed in situ cell, followed by evacuation for 1 h at 1073 K. Then the sample was transferred to the optical part without being exposed to air.

Ga $K$-edge X-ray absorption near-edge structure (XANES) spectra were recorded at room temperature in the transmission mode for high-loading samples (Ga > 1 mol%) or in the fluorescence mode for low-loading samples (Ga ⩽ 1 mol%) at the BL-10B station of Photon Factory, High-Energy Accelerator Research Organization (KEK-PF), Tsukuba, Japan, with a Si(311) channel-cut monochromator [28]. The sample was pretreated with oxygen for 1 h at 1073 K, followed by evacuation for 1 h at 1073 K, and then sealed with a polyethylene film in a dry atmosphere.

Simulation of the Ga $K$-edge XANES spectrum was done similarly as in a previous study [29], based on the assumption that the spectrum comprised two components: gallium in tetrahedral coordination [Ga(Td)] and gallium in octahedral coordination [Ga(Oh)]. Each component was expressed with the sum of one arctangent curve, $T(x)$, for continuum absorption and one combination of Gaussian and Lorentzian curves, $C(x)$, for the white line. The curve-fitting analysis for the XANES spectra, $F(x)$, was carried out using the following equations [30]:

$$F(x) = T(x) + C(x), \tag{2}$$

$$\begin{aligned} T(x) &= T_{Td}(x) + T_{Oh}(x) \\ &= h\left[\frac{1}{2} + \frac{1}{\pi}\tan^{-1}\left(\frac{x - E_{Td}}{B}\right)\right] \\ &\quad + (1-h)\left[\frac{1}{2} + \frac{1}{\pi}\tan^{-1}\left(\frac{x - E_{Oh}}{B}\right)\right], \end{aligned} \tag{3}$$

$$\begin{aligned} C(x) &= C_{Td}(x) + C_{Oh}(x) \\ &= \frac{h_{Td}}{1 + M((x - E_{Td})/w_{Td})^2}\exp\left\{(M-1)(\ln 2)\left(\frac{x - E_{Td}}{w_{Td}}\right)^2\right\} \\ &\quad + \frac{h_{Oh}}{1 + M((x - E_{Oh})/w_{Oh})^2}\exp\left\{(M-1)(\ln 2)\left(\frac{x - E_{Oh}}{w_{Oh}}\right)^2\right\}, \end{aligned} \tag{4}$$

where $x$ represents X-ray energy (eV); $h$, $h_{Td}$, and $h_{Oh}$ represent height; $B$ is a constant fixed at 0.7 eV; $E_{Td}$ and $E_{Oh}$ are the cen-

**Table 1**
Results of photocatalytic methane conversion over gallium oxide and silica-supported gallium oxide[a]

| Entry | Sample | BET specific surface area ($m^2\ g^{-1}$) | Yield of hydrocarbon products ($10^{-2}$ C%[b]) | | | | | | | S[d] (%) | Yield of $H_2$ (μmol) | |
|---|---|---|---|---|---|---|---|---|---|---|---|---|
| | | | Gaseous products | | Adsorbed products[c] | | | | Total yield | | Experimental | Expected[e] |
| | | | $C_2H_6$ | $C_3H_8$ | $C_2H_4$ | $C_2H_6$ | $C_3H_6$ | $C_3H_8$ | | | | |
| 1 | $Ga_2O_3$-K | 2.1 | 16 | 1.0 | 0.1 | 0.1 | n.d. | n.d. | 17 | 96 | 0.11 | 0.18 |
| 2 | $Ga_2O_3$-P | 18 | 13 | 0.3 | 0.4 | 0.5 | n.d. | n.d. | 14 | 95 | 0.07 | 0.15 |
| 3[f] | $Ga_2O_3$-K | 2.1 | 40 | 5.9 | 0.2 | 0.2 | 0.3 | n.d. | 49[g] | 86 | 0.87 | 0.54 |
| 4 | $SiO_2$ | 554 | 0.4 | tr. | n.d. | n.d. | n.d. | n.d. | 0.4 | 93 | n.d. | <0.01 |
| 5 | Ga(0.1)/$SiO_2$ | 499 | 2.3 | n.d. | 0.1 | tr. | n.d. | n.d. | 2.4 | 94 | n.d. | 0.03 |
| 6 | Ga(0.5)/$SiO_2$ | 495 | 2.5 | 0.1 | 0.1 | 0.1 | 0.2 | n.d. | 3.0 | 86 | 0.04 | 0.03 |
| 7 | Ga(1)/$SiO_2$ | 485 | 3.5 | 0.1 | 0.1 | 0.1 | 0.2 | n.d. | 4.1 | 88 | 0.03 | 0.04 |
| 8 | Ga(2)/$SiO_2$ | 436 | 5.2 | 0.1 | 0.2 | 0.2 | 0.2 | tr. | 6.0 | 90 | n.d. | 0.06 |
| 9 | Ga(5)/$SiO_2$ | 402 | 6.2 | 0.1 | 0.3 | 0.5 | 0.2 | 0.1 | 7.2 | 92 | 0.04 | 0.08 |
| 10 | Ga(10)/$SiO_2$ | 389 | 5.8 | 0.1 | 0.3 | 0.5 | 0.3 | 0.1 | 7.0 | 90 | 0.03 | 0.08 |
| 11[f] | Ga(0.1)/$SiO_2$ | 499 | 14 | 1.2 | 0.1 | tr. | n.d. | n.d. | 16 | 94 | 0.17 | 0.16 |
| 12[h] | $Ga_2O_3$-K | 2.1 | 3.8 | 0.1 | 0.3 | 0.1 | 0.2 | n.d. | 4.5 | 90 | 0.09 | 0.05 |
| 13[h] | Ga(0.1)/$SiO_2$ | 499 | 0.2 | n.d. | 0.1 | n.d. | n.d. | n.d. | 0.3 | 73 | n.d. | <0.01 |

[a] Standard condition: reaction temperature was ca. 310 K, sample was 0.2 g, initial methane was 200 μmol, irradiation time was 3 h. Before reaction, the sample was pretreated in oxygen atmosphere at 1073 K for 1 h, followed by evacuation at room temperature for 1 h. $H_2$ was analyzed by TCD (detection limit was 0.03 μmol), hydrocarbons were analyzed by FID (experimental error, <4%).
[b] Based on the initial amount of methane.
[c] The products were obtained after desorption procedure at 573 K for 15 min.
[d] Selectivity of ethane ($S$ = yield of ethane/total yield × 100%).
[e] Calculated from hydrocarbons products.
[f] Irradiation time was 24 h.
[g] $C_2H_4$ ($1.0 \times 10^{-2}$ C%), $C_3H_6$ ($0.4 \times 10^{-2}$ C%) and $C_4H_{10}$ ($1.7 \times 10^{-2}$ C%) were also observed as gaseous products.
[h] Pretreatment prior the reaction was carried out at 773 K. n.d. = not detected. tr. = trace.

ter position of each band (eV); $w_{Td}$ and $w_{Oh}$ are half width at half maximum (eV), and $M$ is the ratio of Gaussian to Lorentzian functions, fixed at 0.85 in this study. The height of each $T(x)$ corresponds to the relative ratio of each gallium species in the sample. The center position of each band, the half-width at half-maximum, and the peak area of each $C(x)$ were determined to simulate the spectrum, and the quantitative ratio of each gallium species was estimated from the best-fitting analysis.

## 3. Results and discussion

### 3.1. Activity for photocatalytic NOCM

Table 1 presents the photocatalytic activities of the unsupported gallium oxide and the silica-supported gallium oxide samples for NOCM. The table confirms that no product was obtained when the reaction was carried out in the dark and/or without photocatalyst. Both $Ga_2O_3$-K and $Ga_2O_3$-P showed high activity for NOCM to produce ethane and hydrogen (entries 1 and 2). The methane conversion was 0.17% on $Ga_2O_3$-K after photoirradiation for 3 h. The yield of ethane in the equilibrium for NOCM was estimated to be 0.0004% based on the thermodynamic equilibrium constant ($K = 3.6 \times 10^{-12}$) at 314 K. Thus, it is clear that the gallium oxide selectively promoted the forward reaction in the photocatalytic NOCM. The apparent quantum yield for NOCM on $Ga_2O_3$-K (entry 1) was roughly estimated to be ca. 0.01% at wavelengths of 220–270 nm.

Even though the $Ga_2O_3$-K had a much lower BET specific surface area, the sample exhibited slightly higher activity than the $Ga_2O_3$-P with a higher specific surface area. XRD patterns revealed that the $Ga_2O_3$-K sample had much higher crystallinity than the $Ga_2O_3$-P sample. This result suggests that, instead of specific surface area, high crystallinity is more important for obtaining high activity for NOCM.

The active semiconductor for the photocatalytic NOCM has not been reported to date. $TiO_2$, a known semiconductor photocatalyst, is not suitable for the reaction, because it can be readily reduced by hydrogen under photoirradiation [1]. However, the gallium oxide semiconductor exhibited high stability under reductive conditions during the reaction. This stability is an important factor required to promote the photocatalytic NOCM. Thus, we emphasize that the gallium oxide is the first semiconductor photocatalyst found to be suitable for promoting NOCM photocatalytically.

The product selectivity for ethane in the total yield of hydrocarbons ($S$ = ethane yield/total yield × 100%) was very high on both $Ga_2O_3$ samples (ca. 95–96%). Other consecutive reactions, such as consecutive coupling to produce longer-chain hydrocarbons and dehydrogenation to produce alkenes from alkanes, proceeded very slowly as minor reactions. These results imply that NOCM shown in Eq. (1) should proceed selectively, at least in the first 3 h of the irradiation; however, the amount of hydrogen produced was lower than that calculated from the amounts of hydrocarbons produced on both unsupported samples after the reaction for 3 h. One possible explanation for this finding is that some type of induction period for hydrogen formation through NOCM may exist, likely due to hydrogen absorption and/or chemisorption on the gallium oxide surface or to the formation of surface gallium hydride species [31–33]. On the other hand, when the reaction was carried out for longer irradiation times, such as 24 h, excess hydrogen was obtained, and the ethane selectivity decreased to 86% (entry 3). Thus, the possibility that during NOCM, the consecutive reactions mentioned above will be further accelerated to increase the production of hydrogen but decrease production of the detectable longer-chain hydrocarbons should be considered.

The amorphous silica exhibited very low photoactivity (entry 4), as reported previously [1–7]. However, methane conversion in the photocatalytic NOCM over the silica still was much higher (ca. 10-fold higher) than the theoretical value calculated from the thermodynamic equilibrium constant (0.0004%).

All of the silica-supported gallium oxide samples exhibited higher yields of hydrocarbons than that of silica (entries 5–10). Similar to the case of the unsupported gallium oxide, all of the silica-supported samples produced ethane as the major product, suggesting that NOCM shown in Eq. (1) was the main reaction. Total yield increased with increasing Ga loading, indicating that the photocatalytic active sites should be related to the Ga species; however, the total yield became constant at loading amounts >5 mol%, as also shown in Fig. 1. No clear relationship between

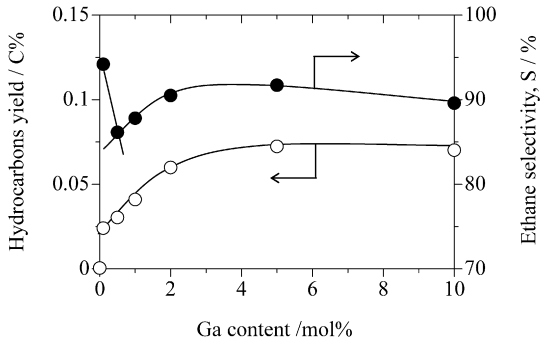


**Fig. 1.** Dependences of hydrocarbons yield (open circle) and ethane selectivity (closed circle) on the Ga content of silica-supported gallium oxide samples.

the BET specific surface area and photoactivity of the samples could be observed, because the major contribution to the surface area should be from the silica support.

The highly dispersed metal oxide species on the supports, such as silica and alumina, have been reported to show higher activity than their corresponding unsupported metal oxides even if they were semiconductors. Thus, this is the first case in which unsupported samples have been shown to have higher activity than silica-supported samples. The unsupported gallium oxide clearly exhibited higher activity than the silica-supported gallium oxide; however, Ga(0.1)/$SiO_2$ had ca. 45-fold greater specific activity per Ga atom compared with the bulk gallium oxide, along with the highest selectivity for ethane formation (94%) among the silica-supported gallium oxide samples studied (entry 5). Even when the detection limits for the minor products were considered, the selectivity was not lower than 92%. Furthermore, high ethane selectivity (ca. 94%) was obtained even after 24 h of irradiation, similar to that obtained after 3-h photoreaction (entries 5 and 11), confirming that NOCM would proceed selectively on Ga(0.1)/$SiO_2$ for a prolonged period. At a reaction time of 3 h, hydrogen was not detected on Ga(0.1)/$SiO_2$, likely due to the detection limit (estimated as 0.03 μmol) of GC (entry 5). However, sufficient hydrogen was obtained after 24 h of photoreaction (entry 11), with the amount of hydrogen obtained almost the same as that expected from NOCM in Eq. (1). Because the total yield of the hydrocarbon products (0.16 C%) obtained on Ga(0.1)/$SiO_2$ after 24 h was similar to that obtained on $Ga_2O_3$-K (0.17 C%) (entries 1 and 11), we can compare the selectivities on these samples. Ethane selectivity among hydrocarbon products was similarly high on these samples. However, it is notable that the amount of hydrogen produced was less than that expected on the unsupported gallium oxide but almost equivalent to that expected on Ga(0.1)/$SiO_2$. These findings indicate that Ga(0.1)/$SiO_2$ exhibited higher selectivity for NOCM, producing both ethane and hydrogen, compared with the unsupported gallium oxide semiconductor photocatalyst.

On Ga(0.5)/$SiO_2$, the ethane selectivity was obviously low, though the yield of hydrocarbons was higher than that on Ga(0.1)/$SiO_2$ (entry 6). But with further increases in Ga content above 0.5 mol%, both product yield and ethane selectivity tended to increase (entries 7–10; also see Fig. 1). The samples containing medium loadings of Ga, such as Ga(0.5)/$SiO_2$ and Ga(1)/$SiO_2$, produced similar amounts of hydrogen as those expected from calculations based on the amounts of hydrocarbons produced (entries 6 and 7). But on the samples with higher Ga loadings ($\geqslant$1 mol%), less hydrogen than expected was produced (entries 7–10). Even when considering the detection limit for hydrogen production (0.03 μmol), the difference between the amount of hydrogen produced and the amount expected from calculations based on the amount of hydrocarbons produced increased from 0.01 to 0.05 μmol with increasing Ga loading (entries 7–10). This is likely due to the presence of aggregated gallium oxide species on the high-loading samples, which can absorb hydrogen, as mentioned above. We confirm the presence of the gallium oxide nanoparticles on high-loading samples in the next section.

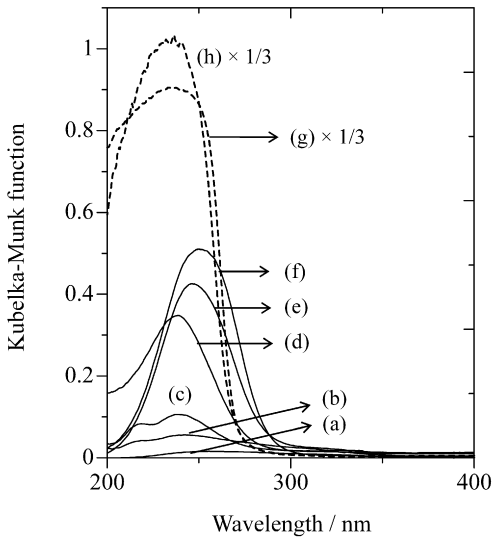


**Fig. 2.** DR UV–visible spectra of the silica-supported gallium oxide samples and unsupported $Ga_2O_3$; (a) Ga(0.1)/$SiO_2$, (b) Ga(0.5)/$SiO_2$, (c) Ga(1)/$SiO_2$, (d) Ga(2)/$SiO_2$, (e) Ga(5)/$SiO_2$, (f) Ga(10)/$SiO_2$, (g) $Ga_2O_3$-K, and (h) $Ga_2O_3$-P. Spectrum intensity of (g) and (h) was multiplied by 1/3.

The effect of the pretreatment temperature was examined on $Ga_2O_3$-K and Ga(0.1)/$SiO_2$. Both of the samples pretreated at higher temperature (1073 K) exhibited much higher activity and higher ethane selectivity than those pretreated at lower temperature (773 K) (entries 1, 5, 12, and 13). These findings suggest that the treated catalyst surface is important for the photocatalytic NOCM. The generation of the active sites on both the unsupported and silica-supported gallium oxide samples may be closely related to the dehydroxylation of hydroxyl groups on the surface.

Under similar conditions, the silica-supported gallium oxide samples exhibited similar activity as has been reported for other silica-based photocatalysts [4], such as silica–alumina, silica-supported zirconium oxide, and silica-supported magnesium oxide. Each of these photocatalysts had the optimum loading amount of metal oxide for high activity in NOCM; however, the activities of silica-supported gallium oxide samples increased with increasing gallium content, with even the bulk gallium oxide exhibiting photocatalytic activity.

### 3.2. Photoexcitation

Fig. 2 shows DR UV–visible spectra of the unsupported gallium oxide samples. Both $Ga_2O_3$-K and $Ga_2O_3$-P exhibited a broad and intense band at below 270 nm, with an estimated band gap of ca. 4.7 eV for both samples. Even though a slight difference was observed on these spectra, these bands can be assigned to $\beta$-phase gallium oxide [24,25].

Fig. 2 also shows DR UV–visible spectra of the silica-supported gallium oxide samples. The sample with the lowest loading amount, Ga(0.1)/$SiO_2$, exhibited a weak, broad band at around 250 nm (Fig. 2a), similar to the spectrum of $SiO_2$ reported previously [2,3]. With increasing Ga loading (to 0.5 and 1 mol%), two absorption bands centered at around 215 and 240 nm appeared (Figs. 2b and 2c). For Ga(2)/$SiO_2$, a broad, large absorption band was observed at around 240 nm with a minor band at around 215 nm (Fig. 2d). For the Ga(5)/$SiO_2$ and Ga(10)/$SiO_2$ samples, only one absorption band centered at 250 nm was observed (Figs. 2e and 2f). These findings indicate that the structure and electronic

state of the gallium species clearly differed between the low-loading and high-loading samples.

Judging from the band position close to that of the bulk gallium oxide samples, the strong band centered at 250 nm should be due to the absorption of gallium oxide nanoparticles or crystallites on silica. On the other hand, the bands centered at 215 and 240 nm can be considered a characteristic of the highly dispersed gallium oxide species on silica support. Because the lowest-loading sample, Ga(0.1)/$SiO_2$, did not exhibit a clear absorption band at ca. 215 nm, the highly dispersed gallium oxide species would exhibit an absorption band at 240 nm. Thus, the weak, broad band at ca. 250 nm for Ga(0.1)/$SiO_2$ would originate from the absorption bands of both the highly dispersed gallium oxide species at 240 nm and the defect on silica at 258 nm [2]. On the other hand, the band at 215 nm would originate from the very small (e.g., 2–5 nm) gallium oxide nanoparticles, as reported previously [34]. The shift of the band for gallium oxide nanoparticles from 215 to 250 nm with increasing Ga content from 0.5 to 10 mol% would correspond to the increase in semiconductor nanoparticle size.

Even though no clear evidence yet exists, we believe that the highly dispersed gallium species exist as isolated gallium oxide monomers (<0.4 nm). This is supported by the photoluminescence findings discussed later. As for the small and large nanoparticles, estimating their sizes is difficult, but because the crystallite size of $Ga_2O_3$-K was found to be 57 nm by XRD and the DR UV spectra of the nanoparticles on silica clearly differed from that of $Ga_2O_3$-K, the nanoparticles on the high-loading samples should be smaller than 50 nm. Because nanoparticles of 2–5 nm have been reported to exhibit an absorption edge at 225–264 nm [34], gallium oxide clusters or small nanoparticles should exist on the medium-loading samples. Based on these results, we can propose that the lowest-loading sample (0.1 mol%) will have highly dispersed gallium oxide monomer species (subnanometer), the medium-loading samples (0.5–2 mol%) will have both highly dispersed gallium species and very small gallium oxide nanoparticles (a few nanometers), and the highest-loading samples (5–10 mol%) will have larger nanoparticles (<50 nm) as the main species.

Regarding band intensity, the unsupported gallium oxide samples clearly were of much greater intensity compared with the silica-supported gallium oxide samples. The strong absorption band for the unsupported gallium oxide means that photoexcited electrons and holes can be formed with high efficiency under UV irradiation. The absorption band for semiconductors is explained by the electron transition from the valence band to the conduction band, that is, electron transfer from $O^{2-}$ to $Ga^{3+}$ in gallium oxide. In contrast, the bands observed for the silica-supported gallium oxides, especially those with low loadings of Ga, were quite different from those for the unsupported gallium oxides, corresponding to the "quantum photocatalysts" [35,36]. These bands can be assigned to localized photoexcitation at isolated sites, such as monomeric gallium species on silica. The excitation process occurs in the Si–O–Ga linkages, as was proposed for highly dispersed metal oxide on silica (i.e., silica-based photocatalysts) [4]. On the silica-supported samples with medium Ga loading having both highly dispersed species and gallium oxide nanoparticles, photoexcitation through the band gap excitation (similar to that on the gallium oxide semiconductor) should be considered along with photoexcitation of monomeric species in the Si–O–Ga linkages.

Photoluminescence spectroscopy has been proposed as a good tool to provide significant information about the photoactive surface sites, especially on the samples with low loadings of metal oxide (<0.1 wt%) [37]. The silica-supported gallium oxide samples exhibited photoluminescence spectra, as shown in Fig. 3. The relatively low-loading samples, Ga(0.1)/$SiO_2$ and Ga(0.5)/$SiO_2$, exhibited phosphorescence spectra with a fine structure (Figs. 3a and 3b), similar to those of silica–alumina, silica-supported zirconium oxide, and silica-supported magnesium oxide [3–6,38], although the present ones were not so clear. Highly dispersed metal oxide species on silica, Si–O–M linkages (M = metal oxide), have been suggested to be the sites responsible for exhibiting the fine structure of the phosphorescence spectra; therefore, the fine structure of the emission spectra would support the presence of highly dispersed gallium oxide species on silica, where photoexcitation with the electron charge transfer is proposed to be localized to the Si–O moiety, as has been suggested for silica-based photocatalysts [4]. On the other hand, the samples with higher Ga loadings exhibited different-shaped phosphorescence spectra compared with the low-loading samples. Ga(2)/$SiO_2$ exhibited a broad emission band centered around 465 nm without the fine structure (Fig. 3c), which can be assigned to gallium oxide nanoparticles [34,39]. These findings are in good agreement with the DR UV–visible spectra of the samples.

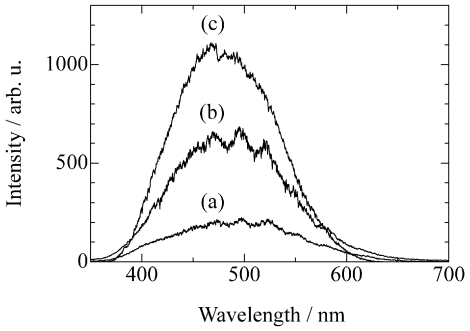


**Fig. 3.** Photoluminescence emission spectra of (a) Ga(0.1)/$SiO_2$, (b) Ga(0.5)/$SiO_2$, and (c) Ga(2)/$SiO_2$. The spectra were recorded at 77 K with the excitation wavelength at 250 nm.

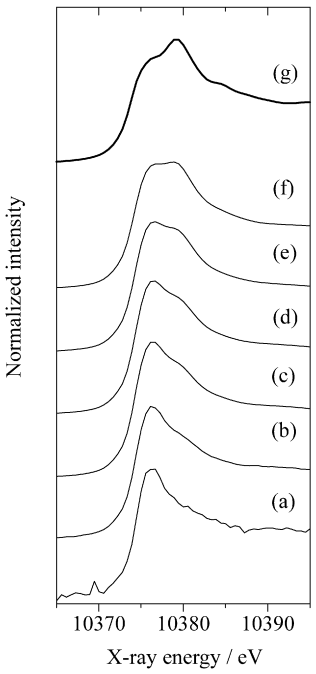


**Fig. 4.** Ga *K*-edge XANES spectra of (a) Ga(0.1)/$SiO_2$, (b) Ga(0.5)/$SiO_2$, (c) Ga(1)/$SiO_2$, (d) Ga(2)/$SiO_2$, (e) Ga(5)/$SiO_2$, (f) Ga(10)/$SiO_2$ samples, and (g) $Ga_2O_3$-K ($\beta$-$Ga_2O_3$).

### 3.3. Local structure

XANES can be used to determine the local structure of the gallium species on the samples both qualitatively and quantitatively [20,29,40]. Fig. 4 shows Ga *K*-edge XANES spectra of the

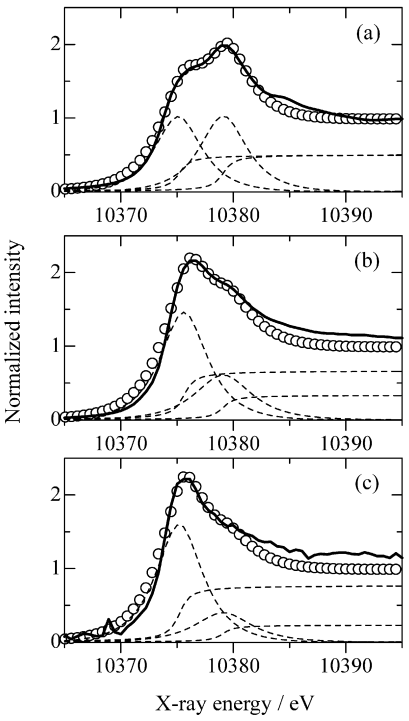


**Fig. 5.** The best results in the curve fitting analysis for XANES spectra of (a) $Ga_2O_3$-K, (b) Ga(1)/$SiO_2$, and (c) Ga(0.1)/$SiO_2$. The solid lines show the experimental spectra. The symbols show the simulated spectra, which are composed of two arctangent functions and two combinations of Gaussian and Lorentzian functions (broken lines).

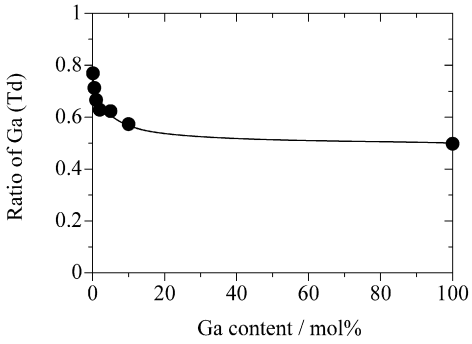


**Fig. 6.** Dependence of Ga(Td) ratio on the Ga content.

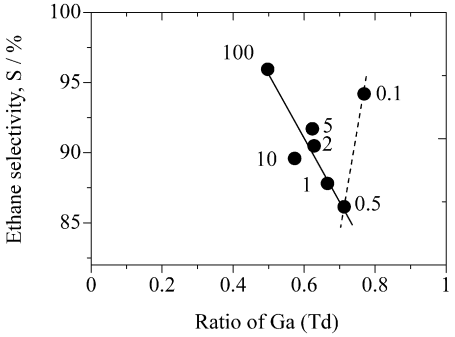


**Fig. 7.** Plot of ethane selectivity versus the ratio of Ga(Td) on the $Ga_2O_3$-K and the silica-supported gallium oxide samples. The numbers show the Ga content (mol%) on the silica-supported samples, and 100 shows the $Ga_2O_3$-K.

unsupported and silica-supported gallium oxide samples. In the unsupported $\beta$-phase gallium oxide, Ga species are known to exist equally in both tetrahedral and octahedral coordinations (1:1 ratio) [41]. The distinguishable peaks at 10,375.2 and 10,379.1 eV on the XANES spectrum of $\beta$-phase gallium oxide have been assigned to Ga(Td), and Ga(Oh), respectively [20,29].

The XANES spectra of the silica-supported gallium oxide samples suggest that the local structure of the gallium species differ between the low-loading and high-loading samples. The highly dispersed gallium oxide species on the low-loading samples would be in tetrahedral coordination, and the gallium oxide nanoparticles on the high-loading samples would consist of tetrahedrally and octahedrally coordinated gallium species.

To obtain the quantitative ratio between Ga(Td) and Ga(Oh), deconvolution analysis of the spectra was carried out by the curve-fitting method mentioned in Section 2. Fig. 5 shows simulated spectra of some samples. Although the samples with low Ga loadings exhibited low spectrum/noise and spectrum/background ratios, making the fitting analysis more difficult, and although unsatisfied parts remained for the 10,370–10,374 eV region and above 10,380 eV on the most of the spectra, the best fitting for each spectrum was determined based on the main features of the target spectrum, as suggested in the literature [42].

The dependence of the Ga local structure on Ga content is represented as the ratio of Ga(Td), as shown in Fig. 6. For comparison, the figure also shows the value for the unsupported $\beta$-phase gallium oxide (100 mol% of Ga content), in which the ratio of Ga(Td) was confirmed to be ca. 50%. With increasing gallium content, the ratio of Ga(Td) species decreased, and the value became close to that of the bulk $\beta$-phase gallium oxide.

Plotting ethane selectivity versus the Ga(Td) ratio of the samples revealed a good relationship between the unsupported gallium oxide samples and the silica-supported ones with medium and high Ga loadings (>0.5 mol%), as shown in Fig. 7. In these samples, the ethane selectivity decreased with increasing Ga(Td) fraction. As discussed above, these silica-supported samples with medium and high Ga loadings contained gallium oxide nanoparticles; therefore, these samples can be expected to behave somewhat similarly to the unsupported gallium oxide samples, especially those with high amounts of gallium oxide nanoparticles. But the photocatalytic properties of the nanoparticles would vary with increases in the Ga(Td) fraction. Our findings suggest that the Ga(Td)-rich nanoparticles would exhibit greater activity for the consecutive reactions. On the other hand, the plot for the lowest-loading sample having the highly dispersed species, i.e., Ga(0.1)/$SiO_2$, was out of line. These results again confirm that the photoexcitation mechanism for these two kinds of photocatalysts—nanoparticles of gallium oxide (semiconductor photocatalyst) and highly dispersed tetrahedral gallium oxide species (quantum photocatalyst)—clearly differ, as was also supported by DR UV–visible and photoluminescence spectra findings. The different excitation mechanisms explain the differences in yield and product selectivity seen in the photocatalytic NOCM.

### 3.4. Active sites

Based on the foregoing results, we proposed the photocatalytic active sites on each type of gallium oxide photocatalyst. The finding of greater ethane selectivity on the lowest-loading sample, Ga(0.1)/$SiO_2$, compared with the medium- and high-loading samples suggests that the highly dispersed tetrahedral gallium oxide species on silica acted as the photoactive sites selectively promoting NOCM. Photoexcitation was localized on the isolated active sites, selectively activating methane molecules. Because the active sites were uniform and well dispersed, other reactions hardly occurred, providing the high selectivity for NOCM.

Together, the unsupported bulk gallium oxide particles, as well as supported nanoparticles existing as major species on Ga(5)/$SiO_2$ or Ga(10)/$SiO_2$, function as a semiconductor photocatalyst. This

catalyst can be efficiently photoexcited, as suggested by the large absorption band. The activity should be high. But the presence of photoexcited electrons and holes on the various surface sites on gallium oxide particles will diminish the reaction selectivity for NOCM and enhance that for other reactions, such as consecutive coupling, dehydrogenation, and coke/carbon formation.

The medium-loading samples, such as Ga(1)/$SiO_2$, were found to contain various photocatalytically active species, such as Ga(Td)-rich gallium oxide small nanoparticles or clusters on silica. Thus, some types of photoactive sites, such as coordinatively unsaturated surface sites, would reduce the selectivity.

## 4. Conclusions

Unsupported and silica-supported gallium oxide were found to promote the photocatalytic NOCM to produce ethane and hydrogen on photoirradiation at around room temperature. Because the conversion exceeded the equilibrium at 314 K, it is obvious that these gallium oxide photocatalysts can selectively promote the forward reaction of the photocatalytic NOCM. This is the advantage of the photocatalytic reaction.

The unsupported gallium oxide as a semiconductor photocatalyst exhibited greater activity than the silica-supported gallium oxide. On the other hand, the highly dispersed tetrahedral species as the quantum photocatalyst on the silica-supported gallium oxide sample of low Ga loading (e.g., 0.1 mol%) was responsible for the high reaction selectivity. Future studies are expected to improve the selectivity of the unsupported gallium oxide photocatalyst and to design more active supported gallium oxide photocatalysts.

## Acknowledgments

The X-ray absorption experiments at the Ga *K*-edge were performed under the approval of the Photon Factory Program Advisory Committee (proposal 2003G248). This work was partially supported by a Grant-in-Aid for Young Scientists (A) (16686045) and a Grant-in-Aid for Scientific Research on Priority Areas (19028023, “Chemistry of Concerto Catalysis”) from the Japanese Ministry of Education, Culture, Sports, Science and Technology (to H.Y.). The authors thank Katsuya Shimura for preparing the unsupported gallium oxide and Naoki Hirabayashi for carrying out the preliminary photoluminescence study.

## References

[1] L. Yuliati, H. Itoh, H. Yoshida, Stud. Surf. Sci. Catal. 172 (2007) 457.
[2] L. Yuliati, M. Tsubota, A. Satsuma, H. Itoh, H. Yoshida, J. Catal. 238 (2006) 214.
[3] H. Yoshida, M.G. Chaskar, Y. Kato, T. Hattori, J. Photochem. Photobiol. A Chem. 160 (2003) 47.
[4] L. Yuliati, T. Hattori, H. Yoshida, Phys. Chem. Chem. Phys. 7 (2005) 195.
[5] H. Yoshida, N. Matsushita, Y. Kato, T. Hattori, Phys. Chem. Chem. Phys. 4 (2002) 2459.
[6] Y. Kato, H. Yoshida, T. Hattori, Chem. Commun. (1998) 2389.
[7] L. Yuliati, T. Hamajima, T. Hattori, H. Yoshida, Chem. Commun. (2005) 4824.
[8] G. Caeiro, R.H. Carvalho, X. Wang, M.A.N.D.A. Lemos, F. Lemos, M. Guisnet, F.R. Ribeiro, J. Mol. Catal. A 255 (2006) 131.
[9] R.L. van Mao, J. Yao, L.A. Dufresne, R. Carli, Catal. Today 31 (1996) 247.
[10] P. Mériaudeau, C. Naccache, Catal. Today 31 (1996) 265.
[11] A. Raj, J.S. Reddy, R. Kumar, J. Catal. 138 (1992) 518.
[12] Y.K. Park, K.Y. Park, S.I. Woo, Catal. Lett. 26 (1994) 169.
[13] A. Corma, F. LLopis, P. Viruela, C. Zicovich-Wilson, J. Am. Chem. Soc. 116 (1994) 134.
[14] E. Lalik, X. Liu, J. Klinowski, J. Phys. Chem. 96 (1992) 805.
[15] V.R. Choudhary, A.K. Kinage, Zeolites 15 (1995) 732.
[16] M. Kang, C.-T. Lee, J. Mol. Catal. A 150 (1999) 213.
[17] E. Kikuchi, K. Yogo, Catal. Today 22 (1994) 73.
[18] Y. Li, J.N. Armor, J. Catal. 145 (1994) 1.
[19] J.N. Armor, Catal. Today 31 (1996) 191.
[20] K. Shimizu, M. Takamatsu, K. Nishi, H. Yoshida, A. Satsuma, T. Tanaka, S. Yoshida, T. Hattori, J. Phys. Chem. B 103 (1999) 1542.
[21] A. Satsuma, Y. Segawa, H. Yoshida, T. Hattori, Appl. Catal. A 264 (2004) 229.
[22] A. Kudo, I. Mikami, J. Chem. Soc. Faraday Trans. 94 (1998) 2929.
[23] T. Yanagida, Y. Sakata, H. Imamura, Chem. Lett. 33 (2004) 726.
[24] Y. Hou, X. Wang, L. Wu, Z. Ding, X. Fu, Environ. Sci. Technol. 40 (2006) 5799.
[25] Y. Hou, L. Wu, X. Wang, Z. Ding, Z. Li, X. Fu, J. Catal. 250 (2007) 12.
[26] L. Yuliati, H. Itoh, H. Yoshida, Chem. Phys. Lett. 452 (2008) 178.
[27] H. Yoshida, C. Murata, T. Hattori, J. Catal. 194 (2000) 364.
[28] M. Nomura, A. Koyama, KEK Report 89-16 (1989) 1.
[29] K. Nishi, K. Shimizu, M. Takamatsu, H. Yoshida, A. Satsuma, T. Tanaka, S. Yoshida, T. Hattori, J. Phys. Chem. B 102 (1998) 10190.
[30] Y. Kato, K. Shimizu, N. Matsushita, T. Yoshida, H. Yoshida, A. Satsuma, T. Hattori, Phys. Chem. Chem. Phys. 3 (2001) 1925.
[31] E.A. Gonzales, P.V. Jasen, A. Juan, S.E. Collins, M.A. Baltanás, A.L. Bonivardi, Surf. Sci. 575 (2005) 171.
[32] B. Xu, B. Zheng, W. Hua, Y. Yue, Z. Gao, J. Catal. 239 (2006) 470.
[33] E.A. Pidko, V.B. Kazansky, E.J.M. Hensen, R.A. van Santen, J. Catal. 240 (2006) 73.
[34] G. Sinha, D. Ganguli, S. Chaudhuri, J. Phys. Condens. Matter 18 (2006) 11167.
[35] H. Yoshida, Curr. Opin. Solid Mater. Sci. 7 (2003) 435.
[36] H. Yoshida, Catal. Surv. Asia 9 (2005) 1.
[37] M. Anpo, M. Che, Adv. Catal. 44 (2000) 119.
[38] Y. Kato, H. Yoshida, T. Hattori, Phys. Chem. Chem. Phys. 2 (2000) 4231.
[39] X. Xiang, C.-B. Cao, H.-S. Zhu, J. Cryst. Growth 279 (2005) 122.
[40] K. Shimizu, M. Takamatsu, K. Nishi, H. Yoshida, A. Satsuma, T. Hattori, Chem. Commun. (1996) 1827.
[41] S. Geller, J. Chem. Phys. 33 (1960) 676.
[42] S. Yoshida, T. Tanaka, in: Y. Iwasawa (Ed.), X-ray Absorption Fine Structure for Catalysts and Surfaces, World Scientific, Singapore, 1996, p. 304.